POWDER SINTERING AND CHARACTERIZATION OF BIOMEDICAL POROUS TiNb ALLOY

Y.H. LI*, N. CHEN, H.L. ZHANG
School of Materials Science and Engineering, Shenyang Ligong University, Shenyang, P. R. China

Porous titanium alloys have attracted considerable attention in the field of hard tissue implants owing to the biocompatibility and low Young's modulus. Porous Ti-49Nb alloy was prepared by powder metallurgy approach from pure TiH_2 and Nb powders. NH_4HCO_3 powders were used as space holder. The relationships between mechanical property, corrosion behavior and porous structure of the sintered porous Ti-49Nb alloys were investigated. Pore size, porosity, morphology and interconnectivity can be altered by the adding amount of space holder. Furthermore, the tailored Young's modulus and compressive strength decrease significantly with the increasing porosity. Corrosion potential decreases whereas corrosion current density increases with the increasing porosity. Pore size, Young's modulus and compressive strength of porous Ti-49Nb alloy with porosity of 38.9~60.2% meet the porous structure and mechanical properties requirements of porous biomaterials, suggesting it is an appropriate implant candidate for cancellous bone.

(Received January 25, 2018; Accepted May 18, 2018)

Keywords: TiNb alloy, Porosity, Mechanical property, Electrochemical behavior

1. Introduction

The exceptional characteristics of titanium alloys have led to a variety of applications in aerospace, medical and other fields. Solid titanium alloys have attracted much attention in the field of load-bearing implants due to the combination of high strength and ductility, good corrosion resistance, etc [1-3]. But the intrinsic Young's moduli of traditional titanium alloys are significantly higher than those of cortical and cancellous bones [2, 3]. This Young's modulus incompatibility may cause stress shielding effect and osteoporosis [1-3]. Furthermore, allergic reaction and neurological disorder have been reported to be associated with the cytotoxicity of incompatible metallic elements like aluminum, vanadium, nickel, etc. [3]. Therefore, new generation of near β type titanium alloys with low Young's modulus have been developed by choosing some non-toxic and β stabilizing metallic elements such as niobium, zirconium, tantalum, molybdenum, etc. [3]. TiNb alloy is superior to other β-type titanium alloys with respect to appropriate Young's modulus, good osteogenesis and other biocompatibilities [4-11].

All implanted alloys will be subjected to corrosion because of the aggressive chloride ions in the human body fluid. Consequently, corrosion resistance is of great significance to biomedical metallic implant because it may determine the service lifetime [1, 12-14].

As a main existing form of mature bone, cancellous bone consists of connected network of rods and plates, showing porous structure. This cellular structure permits the transportation of body fluid and nutrients [15, 16].

Fabrication of porous material by introduction of pores is an effective and attractive measure to lower the Young's modulus of metallic implant candidate, mimicking the porous structure of cancellous bone tissue [2, 17-20].

Recently, there are some investigations regarding fabrication, mechanical behavior and biocompatibility of porous Ti-Nb alloys designed for hard tissue implant applications. Several methods for the fabrication of porous TiNb alloys have been reported, including powder metallurgy (PM), gelcasting, selective laser melting (SLM) and hot pressing. Porous Ti-(25-45)Nb

*Corresponding author: yhlicn@163.com

alloys were prepared by PM approach from elemental Ti and Nb powders [9, 19-24]. Porous Ti-(10~35)Nb alloys were produced using gelcasting route under vacuum condition [25]. SLM, an additive manufacturing method and hot pressing were employed to fabricate porous Ti-40Nb alloys [26].

The investigations into the influence of porosity on the corrosion behavior of Ti-39Nb alloy indicated that corrosion behavior of the alloy with porosity below 15% was comparable with a compact one while the apparent corrosion attack was proved in the alloy with porosity of 15% or higher [27].

The mechanical properties of porous TiNb alloys have been investigated by compressive tests. Young's modulus and compressive strength of Ti-(10~45)Nb alloys with porosity of 17%~80% were in the range of 33GPa~1.5GPa and 968MPa~10MPa, respectively [19-26]. Young's modulus of porous Ti-40Nb alloy was predicted by finite element analysis, and comparable to the experimental result [22].

In vitro investigations like cell proliferation, MTT assay, mineralization nodules and so on were assessed for porous Ti-(25~40)Nb alloys. The results demonstrated that porous Ti-Nb alloys exhibited good biocompatibility, being similar to that of titanium [9, 24].

To the authors' knowledge, there is little literature regarding fabrication and properties of porous β type Ti-49Nb alloy with higher Nb content. In this work, porous Ti-49Nb alloys are fabricated by PM method under protection of flow argon from TiH_2 and Nb powders. TiH_2 is used as the raw powders and also the pore former in a metallurgical process. NH_4HCO_3 powders are used for space holder material to adjust the pore size, morphology, porosity and then mechanical behavior and corrosion behavior. The primary purpose of this work is to investigate the relationships between the mechanical property, corrosion behavior and porous structure of the sintered porous Ti-49Nb alloys.

2. Experimental

2.1 Preparation of porous TiNb alloy

PM approach was employed to fabricate porous Ti-49Nb alloy using space holder technique. Pure TiH_2 (≤150 μm) and Nb (≤150 μm) powders weighted to the nominal composition of Ti-49wt.% Nb were blended for 24 h. The blended metallic powders were mixed with NH_4HCO_3 powders (≤300 μm) for 8h, which served as temporary space holder materials. The amount of space holder was 12.5%, 25.0% and 37.5 wt.% in this case, respectively.

The mixed powders were cold pressed into green rod shaped compacts and placed into a tube furnace under the protection of flowing argon. The green compacts were heated to 473K for 2 h to remove ammonium bicarbonate and then heated to 1073K for 1h to dehydrogenate TiH_2 into Ti and hydrogen. Subsequently, the samples were heated to 1473K and kept for 5h followed by air cooled to conduct sintering process. Heating rate was controlled at 3K/min during all heating process.

2.2 Characterization

X-ray diffraction (XRD) measurements were performed to determine the phase constituents of the mixed TiH_2-Nb powders and the sintered porous Ti-49Nb alloy on Rigaku D/max. Scanning electron microscopy (SEM) investigations were carried out to observe the pore structure of porous Ti-Nb alloy on Hitachi S3400.

Mechanical behavior of porous Ti-49Nb alloy was investigated by compressive test on cylindrical samples (Φ10mm×12mm) of each porosity level. The Young's modulus and compressive strength of the porous alloy were measured using a universal mechanical testing machine at crosshead speed of 1mm/min.

A conventional three-electrode system was used for the electrochemical corrosion measurements. The spark cut and carefully rinsed porous Ti-49Nb alloy samples were used as the working electrode, platinum sheet as the counter electrode and a saturated calomel electrode (SCE) as the reference electrode, respectively. The scanning rate of potential was set at 1mV/S. All the measurements were conducted in the electrolyte of naturally aerated 0.9wt.% NaCl solution at ambient temperature of about 298K.

3. Results and discussion

3.1 Analysis of phases

XRD patterns shown in Fig.1 (a) confirm that the mixed powders are pure TiH_2 and Nb powders. As presented in Fig.1 (b), XRD results of the porous Ti-49Nb alloy sintered by adding 37.5% NH_4HCO_3 reveal that only diffraction peaks representing β titanium phase can be detected. The experimental results are in accord with the phase compositions of Ti-49Nb alloy depicted in the phase diagram [28]. The results confirm that the addition and decomposition products of NH_4HCO_3 have no influences on the phase constituents of the sintered porous Ti-49Nb alloy.

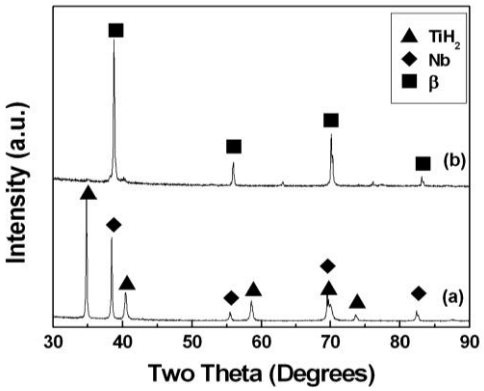

Fig. 1. XRD patterns (a) the mixed TiH_2 and Nb powders (b) porous Ti-49Nb alloy sintered with 37.5% space holder agent.

According to the Ti-Nb phase diagram, there is no liquid phase within the sintering temperature range. Consequently, solid phase diffusion becomes the primary densification mechanism during the sintering process of the green compact. As a result, Nb powders diffuse into the Ti matrix, leading to the formation of β phase.

3.2 Porous structure and pore characteristics of porous Ti-49Nb alloys

Porosity (P) of the sintered porous Ti-49Nb alloys was measured according to the followi ng equation (1):

$$P = [1 - \rho/\rho_s] \times 100\% \quad (1)$$

where ρ and ρ_s ($5.94 g/cm^3$) denote the density of the porous and solid (porosity free) Ti-49Nb alloys, respectively. Table 1 depicts the correlation between porosity of the sintered porous alloy and the addition amount of NH_4HCO_3. Porosity of Ti-49Nb alloy tends to increase noticeably from 23.7% to 38.9% and 60.2% with increasing NH_4HCO_3 addition from 12.5% to 25.0% and 37.5%, respectively.

Fig. 2 presents the SEM photographs for porous structure of porous Ti-49Nb alloys sintered with different amount of space holder material. As could be seen from Fig.2(a), the pore structure is characterized by macro-pores and micro-pores in the porous alloys sintered with 12.5% amount of NH_4HCO_3. The former are some irregular shaped macro-pores with pore size larger than around 100 μm, which is highlighted by ellipse. These macro-pores are distributed homogeneously in the matrix. The latter are many near-circular micro-pores with pore size smaller than about 30 μm, which is highlighted by rectangle. These isolated micro-pores are distributed unevenly inside and on the walls of the macro-pores. As shown in Fig. 2(b), the pore structure of

the porous alloy sintered with 25.0% amount of NH_4HCO_3 is similar to that shown in Fig. 2(a) except that the pore size is enhanced with the increasing amount of space holder material. As displayed in Fig.2(c), the number and interconnectivity of open pores in the porous titanium alloy are enhanced significantly when the amount of added space holder material increases to 37.5%. The roughened and irregular shaped surfaces of pores are associated with the irregular shape of the space holder NH_4HCO_3 powders. The sintered porous Ti-49Nb alloy exhibits a complex porous structure with interconnected pores, resembling that of cancellous bone.

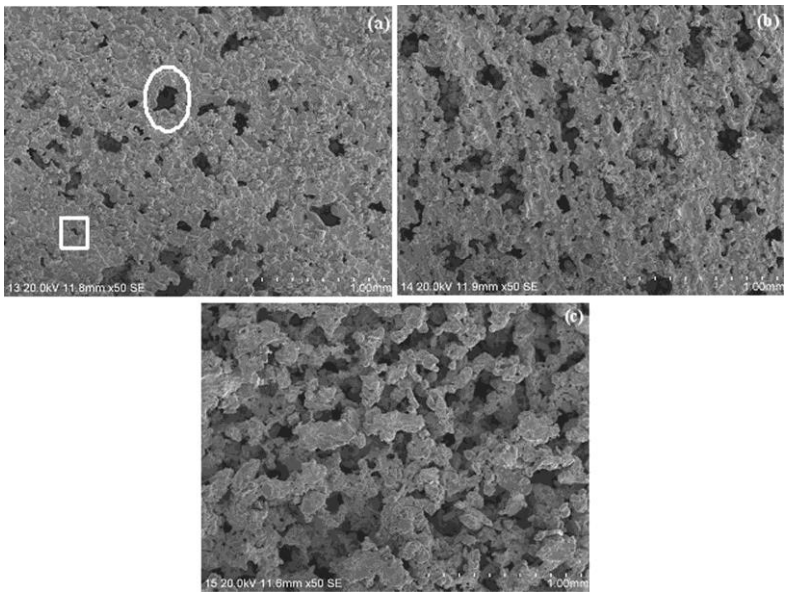

Fig. 2. SEM images of pore structure for porous Ti-49Nb alloys fabricated by powder sintering with different amount of adding space holder agent (a) 12.5%, (b) 25.0%, (c) 37.5%.

The established reports reveal that macro-pores and micro-pores may play important roles in the enhancement of biocompatibility. The macro-pores characterized by interconnected open structure could facilitate the osteoinduction and osteointegration, ingrowth of bone tissue, transportation of human body fluid and nutrients. The micro-pores on the walls and inner the macro-pores could allow the impregnation of bioactive coating like hydroxyapatite [29].

Table 1 demonstrates the average macro-pore size of the sintered porous Ti-49Nb alloys determined using image analysis on each porosity level. It increases gradually from 116 μm to 135 μm and 219μm with the increase of NH_4HCO_3 addition from 12.5% to 25.0% and 37.5%, respectively. Pore structures including pore size and interconnectivity would exert significant influences on bone tissue regeneration. It is recognized that open pore with average size bigger than about 100 μm is appropriate for bone tissue ingrowth, body fluid and nutrients transportation, and then implant fixation [16, 29]. Consequently, Pore characteristics of porous Ti-49Nb alloys with porosity bigger than 38.9% meets the preliminary pore structure requirement of porous implants.

Table 1. Porosity and average pore size of porous TiNb alloy sintered with different amount space holder agent.

Amount of space holder (wt.%)	Porosity (%)	Average pore size (μm)
12.5	23.7±2.8	116±5
25.0	38.9±3.5	135±6
37.5	60.2±3.9	219±8

As far as the pore-forming mechanism of porous Ti-49Nb alloy is concerned, the macro-pores primarily derive from the decomposition of NH_4HCO_3 powders. Moreover, the micro-pores may originate from the evolution of hydrogen which comes from the dehydrogenization of TiH_2, the volatilization of impurities and the gap between powders during alloying and densifying process of the green compacts.

3.3 Mechanical behavior of porous Ti-49Nb alloys

Fig. 3 shows the compressive nominal stress-strain curves of porous Ti-49Nb alloys with various porosities between 23.7% and 60.2%. The curves show a three-stage deformation behavior. It starts with an initial linear elastic stage in which pore walls would deform elastically. The second is a continuous yielding and hardening stage till a plateau in which the stress would increase up to the maximum, i.e. compressive strength. Pore walls would buckle or bend plastically in this stage. The last is fracture stage in which pore walls would be densified and then collapse. Compressive strength decreases dramatically from 183.7±16.1MPa to 87.3±12.6MPa and 37.1±7.5MPa when porosity is enhanced from 23.7% to 38.9% and 60.2%, respectively. The distinct decrease in effective loading area is responsible for the remarkable weakening of the strength. Compressive strength of porous Ti-49Nb alloys is comparable to that of cortical and cancellous bones (2-180MPa) [15, 16].

Furthermore, the Young's modulus of porous Ti-49Nb alloys measured by the slope in the initial linear elastic stress-strain region decreases from 4.3±0.6GPa to 3.1±0.4GPa and 1.9±0.3GPa with the increase of porosity. Stiffness of porous Ti-49Nb alloy matches that of cancellous bone [15, 16].

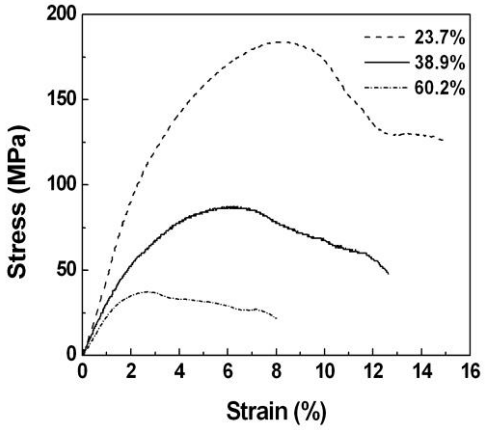

Fig. 3. Compressive nominal stress-strain curves of porous Ti-49Nb alloys with different porosity.

3.4 Electrochemical behavior of porous Ti-49Nb alloys

The corrosion resistance is critical to the application of metallic biomaterial because its possible degradation is correlated to the interaction with the body fluid containing aggressive chloride ions. Corrosion behavior of titanium alloys is commonly evaluated by electrochemical tests.

Fig.4 depicts the electrochemical polarization curves of porous Ti-49Nb alloys with different porosity in physiological solution (0.9% NaCl). All the anodic polarization portions change gradually from Tafel region into passive state with characteristics of self-passivation, manifesting similar behavior. There is no apparent breakdown sign of the passivation in the scanned potential range. Table 2 summarizes the corrosion potential (E_{corr}) and corrosion density current (i_{corr}), which is extrapolated from the cathodic and anodic branches in the Tafel region.

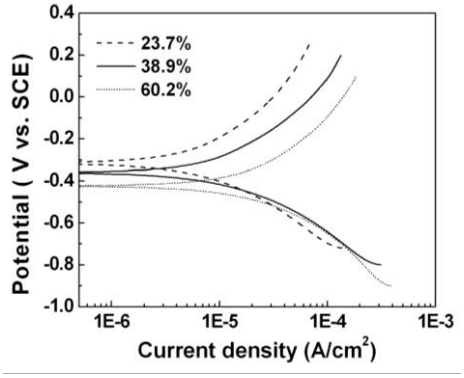

Fig. 4. Polarization curves of porous Ti-49Nb alloys with different porosity in 0.9% NaCl solution.

It can be observed clearly that E_{corr} value shifts towards the noble direction while i_{corr} value has a downward trend for the porous Ti-49Nb alloy with the decrease of porosity. These variation tendencies indicate the corrosion resistance is enhanced with the decrease of porosity. It is similar to that of porous Ti-39Nb alloy or porous NiTi alloy [30]. Accordingly, the results indicate a significant influence of porous structure on the corrosion resistance of TiNb alloy.

Table 2 Corrosion potential and corrosion current density values of the sintered porous Ti-49Nb alloys with different porosity

Porosity (%)	Corrosion potential (mV)	corrosion current density (μA/cm^2)
23.7	-312±25	4.24±0.05
38.9	-368±28	6.63±0.06
60.2	-426±32	9.32±0.09

It is well recognized that the complex pore structure and the larger actual surface area exposed to the physiological solution account for the degradation of corrosion resistance of porous alloys compared with the solid counterparts [27, 30]. Porous structure of porous Ti-49Nb alloy is characterized by the enhancement of pore size and interconnectivity with the increase of porosity. As a result, more electrolyte solution would be trapped in the big and interconnected pores in the high porosity sample, leading to crevice corrosion [31, 32].

In generally, the electrochemical reactions between the passive film spontaneously formed on the surface and chloride ions in the aqueous solution contribute to the degradation of corrosion resistance of titanium alloys [28]. Porous Ti-49Nb alloy with higher porosity is more susceptible to be corrosion attacked because the roughened pore surface and larger surface area exposed to solution would provide more possible electrochemical reaction sites for crevice corrosion. Therefore, the porous Ti-49Nb alloy is less corrosion resistant than the solid one.

It should be pointed out that as an optional solution, deposition of hydroxyapatite coating on the surface of porous Ti-Nb alloy may enhance the corrosion resistance and alleviate the corrosion attack.

4. Conclusions

Based on the studies of the dependence of porous structure, mechanical property and corrosion behavior of the sintered porous Ti-49Nb alloys on space holder content, the following

conclusions can be reached:

a) Pore characteristics including pore size, morphology and porosity can be adjusted by the amount of space holder NH_4HCO_3.

b) The tailored Young's modulus and compressive strength decrease with the increasing porosity.

c) Corrosion resistance degrades with the increasing porosity.

d) Porous Ti-49Nb alloys with porosity in the range of 38.9~60.2% fulfill the major demands of biomaterials with respect to pore characteristics and mechanical properties for use of bone implants.

Acknowledgements

The work was financially supported by the Scientific Research Project of Education Department of Liaoning Province of China (LG201612) and Opening Foundation for Key Discipline in Shenyang Ligong University (4771004kfx16)

References

[1] M. Geetha, A.K. Singh, R. Asokamani, A.K. Gogia, Prog. Mater. Sci. **54**, 397 (2009).
[2] Y. Li, C. Yang, H. Zhao, S. Qu, X. Li, Y. Li, Materials **7**, 1709 (2014).
[3] M. Niinomi, M. Nakai, J. Hieda, Acta Biomater. **8**, 3888 (2012).
[4] E. Eisenbarth, D. Velten, M. Müller, R. Thull, J. Breme, Biomaterials **25**, 5705 (2004).
[5] Y. Bai, Y. Deng, Y. Zheng, Y. Li, R. Zhang, Y. Lv, Q. Zhao, S. Wei, Mater. Sci. Eng. C **59**, 565 (2016).
[6] C. M. Lee, C. P. Ju, J. H. C. Lin, J. Oral Rehabilitation **29**, 314 (2002).
[7] D. R. Santos, M. S. Pereira, C. A. A. Cairo, M. L. A. Graca, V. A. R. Henriques, Mater. Sci. Eng. A **472**, 193 (2008).
[8] D. Zhao, K. Chang, T. Ebel, M. Qian, R. Willumeit, M. Yan, F. Pyczak, J. Mech. Behav. Biomed. Mater. **28**, 171 (2013).
[9] D. P. de Andrade, L. M. R.de Vasconcellos, I. C. S. Carvalho, L. F. de B. P. Forte, E. L. de S. Santos, R. F. do Prado, D. R. dos Santos, C. A. A. Cairo, Y. R. Carvalho, Mater. Sci. Eng. C **565**, 38 (2015).
[10] R. E. McMahon, J. Ma, S. V. Verkhoturov, D. Munoz-Pinto, I. Karaman, F. Rubitschek, H. J. Maier, M. S. Hahn, Acta Biomater. **8**, 2863 (2012).
[11] A. Terayama, N. Fuyama, Y. Yamashita, I. Ishizaki, H. Kyogoku, J. Alloys Compd. **577S**, 408 (2013).
[12] Y. Bai, Y. Wang, Y. Cheng, F. Deng, Y. Zheng, S. Wei, Mater. Sci. Eng. C **31**, 702 (2011).
[13] R. Godley, D. Starosvetsky, I. Gotman, J. Mater. Sci. Mater. Med.**17**, 63 (2006).
[14] T. Hanawa, Sci. Technol. Adv. Mater. **3**, 289 (2002).
[15] L. J. Gibson, J. Biomech. **18**, 317 (1985).
[16] W. Suchanek, M. Yoshimura, J. Mater. Res. **13**, 94 (1998).
[17] Y. H. Li, R. B. Chen, G. X. Qi, Z. T. Wang, Z. Y. Deng, J. Alloys Compd. **485,** 215 (2009).
[18] X. Wang, Y. Li, J. Xiong, P. D. Hodgson, C. E. Wen, Acta Biomater. **5,** 3616 (2009).
[19] K. Zhuravleva, A. Chivu, A. Teresiak, S. Scudino, M. Calin, L. Schultz, J. Eckert, A. Gebert, Mater. Sci. Eng. C **33**, 2280 (2013).
[20] C. S. S. de Oliveira, S. Griza, M. V. de Oliveira, A. A. Ribeiro, M. B. Leite, Powder Technol. **281**, 91 (2015).
[21] X. J. Wan, Trans. Nonferrous. Met. Soc. China **21**, 13 (2011).
[22] K. Zhuravleva, R. Müller, L. Schultz, J. Eckert, A. Gebert, M. Bobeth, G. Cuniberti, Mater. Design **64**, 1 (2014).
[23] R. Schmidt, S. Pilz, I. Lindemann, C. Damm, J. Hufenbach, A. Helth, D. Geissler , A. Henss, M. Rohnke, M. Calin, M. Zimmermann, J. Eckert, M. H. Lee, A. Gebert, Powder Technol. **322**, 393 (2017).
[24] J. Xu, X. J. Weng, X. Wang, J. Z. Huang, C. Zhang, H. Muhammad, X. Ma, Q. D. Liao, Plos One **8**, e79289 (2013).

[25] D. Yang, Z. Guo, H. Shao, X. Liu, Y. Ji, Procedia Eng. **36**, 160 (2012).
[26] K. Zhuravleva, M. Bönisch, K. G. Prashanth, U. Hempel, A. Helth, T. Gemming, M. Calin, S. Scudino, L. Schultz, J. Eckert, A. Gebert, Materials **6**, 5700 (2013).
[27] J. Fojt, L. Joska, J. Málek: Corro. Sci. **71,** 78 (2013).
[28] A. Cremasco, W. R. Osório, C. M. A. Freire, A. Garcia, R. Caram, Electrochimica Acta **53,** 4867 (2008).
[29] M. Metikos-Hukovic, E. Tkalcec, A. Kwokal, J. Piljac, Surf. Coat. Technol. **165**, 40 (2003).
[30] X. T. Sun, Z. X. Kang, X. L. Zhang, H. J. Jiang, R. F. Guan, X. P. Zhang, Electrochimica Acta **56**, 6389 (2011).
[31] Y. H. Li, G. B. Rao, L. J. Rong, Y. Y. Li, Mater. Lett. **57**, 448 (2002).
[32] F. Xie, X. He, S. Cao, M. Mei, X. Qu, Electrochimica Acta **105**, 121 (2013).